

INTEGRATED AND FIBRE OPTICS

PACS numbers: 42.81.–i; 42.55.Wd
DOI: 10.1070/QE2011v041n07ABEH014522

Steady-state heating of active fibres under optical pumping

V.V. Gainov, R.I. Shaidullin, O.A. Ryabushkin

***Abstract*. We have measured the temperature in the core of rare-earth-doped optical fibres under lasing conditions at high optical pump powers using a fibre Mach – Zehnder interferometer and probe light of wavelength far away from the absorption bands of the active ions. From the observed heating kinetics of the active medium, the heat transfer coefficient on the polymer cladding – air interface has been estimated. The temperature of the active medium is shown to depend on the thermal and optical properties of the polymer cladding.**

Keywords: *fibre laser, active optical fibre, fibre Mach – Zehnder interferometer, temperature of the active medium, heat transfer coefficient, coaxial heating model.*

High-power single-mode rare-earth-doped silica fibre lasers and amplifiers are used in a variety of industrial applications, materials processing, optical communication systems, medicine and science [1]. The diversity of their application areas is due to the considerable output power, high beam quality ($M^2 < 1.2$) and other unique optical emission characteristics of such lasers. It was shown theoretically and experimentally as early as 20 years ago [2] that, owing to their properties, fibre lasers can be used as light sources providing tens and hundreds of watts of power in continuous mode. It is worth noting the high optical damage threshold of silica glass (tens of gigawatts per square centimetre at wavelengths near 1 μm); the large surface area to volume ratio of fibres, which ensures rapid heat removal under natural conditions; and light guiding, which enables an effective overlap of the pump field and active medium. Advances in the technology and fabrication of both active fibres and fibre components made it possible to reach the highest optical power among single-mode cw solid-state lasers: 10 kW [3].

A basic structural component of fibre lasers is an active silica fibre with a core doped with rare-earth ions (Yb^{3+}, Er^{3+}, Tm^{3+}, Nd^{3+} and others). The active medium is pumped by multimode light from high-power, efficient semiconductor laser diodes coupled to a multimode fibre.

The main physical mechanisms that limit the output power of fibre lasers are the thermal degradation of the active fibre and the onset of nonlinear effects [4]. This paper examines effects related to the optical pumping-induced heating of active media.

The most widespread types of active fibres are few-mode and single-mode fibres doped with Yb^{3+} (gain in the range 975 – 1100 nm) or doped with Er^{3+} and sensitised by ytterbium ions for light amplification in the telecom window 1535 – 1600 nm. Figure 1 shows a simplified energy level diagram of an active medium with schematic representation of different excitation relaxation processes.

At the wavelengths indicated in Fig. 1, the difference between the pump photon energy ($\lambda_p = 920 - 970$ nm) and laser photon energy ($\lambda_{laser} = 1030 - 1100$ nm) in ytterbium-doped gain media, which is converted to heat, ranges from 5 % to 10 %. In Yb – Er codoped fibre, almost half of the absorbed pump power is converted to heat through the rapid nonradiative transition $^4I_{11/2} \rightarrow {}^4I_{13/2}$ ($\tau \approx 30$ μs [7]), which considerably limits the laser output power (the highest output power of cw Yb – Er codoped fibre lasers achieved to date is 297 W [8]).

In addition, considerable heating of active fibre may influence its waveguiding properties through changes in both its refractive index profile and the properties of the polymer material the multimode cladding is made of. A rise in the temperature of the active medium leads to an increase in the homogeneous broadening of laser transition and, accordingly, to changes in absorption and emission cross sections and a reduction in pump efficiency [9, 10]. For example, Brilliant and Lagonik [10] experimentally demonstrated a 20 % decrease in the output power of an ytterbium fibre laser on heating from 0 to 90 °C.

Issues pertaining to thermal effects in active fibres are now receiving a great deal of attention [11 – 17]. Various approaches to cooling high-power (kilowatt) lasers have been described in the literature [12, 13], and a number of models for thermal effects induced in fibre by high-power optical pumping have been proposed using a steady-state heat equation [11, 14 – 16].

One of the first reviews concerned with approaches to

V.V. Gainov, R.I. Shaidullin IRE-Polus Research and Technology Association, pl. Vvedenskogo 1, 141190 Fryazino, Moscow region, Russia; Moscow Institute of Physics and Technology (State University), Institutskii per. 9, 141700 Dolgoprudnyi, Moscow region, Russia; e-mail: vg254@rambler.ru, unknownmipter@gmail.com;
O.A. Ryabushkin IRE-Polus Research and Technology Association, pl. Vvedenskogo 1, 141190 Fryazino, Moscow region, Russia; Moscow Institute of Physics and Technology (State University), Institutskii per. 9, 141700 Dolgoprudnyi, Moscow region, Russia; V.A. Kotel'nikov Institute of Radio Engineering and Electronics (Fryazino Branch), Russian Academy of Sciences, pl. Vvedenskogo 1, 141190 Fryazino, Moscow region, Russia;
e-mail: roa228@mail.ru

Received 29 November 2010; revision received 18 May 2011
Kvantovaya Elektronika **41** (7) 637 – 643 (2011)
Translated by O.M. Tsarev

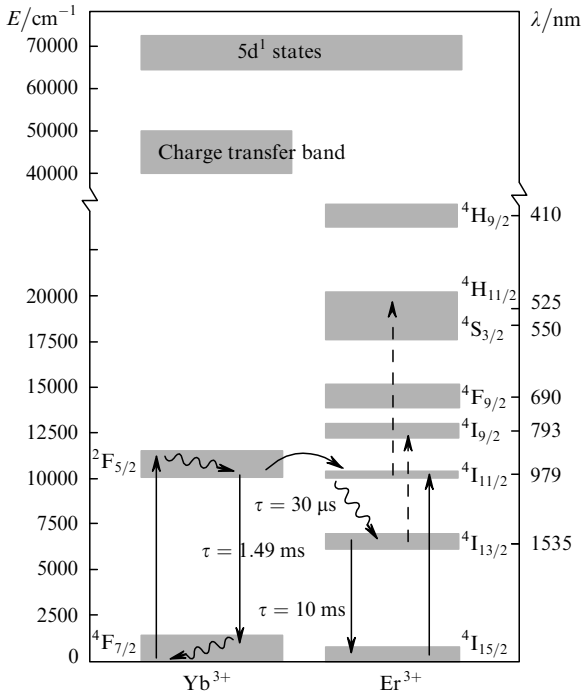

Figure 1. Energy level diagram of the Yb^{3+} and Er^{3+} ions in silica glass [5–7]. The solid straight arrows represent radiative transitions, the wavy arrows represent nonradiative transitions, the dashed arrows show possible upconversion channels, and the curved arrow represents nonradiative excitation transfer between the ytterbium and erbium ions in Yb^{3+}/Er^{3+} codoped fibres. The charge transfer zone in doped silica glass results from the overlap of the outer electron shells of the dopants and oxygen.

raising the output power of fibre lasers to the kilowatt level [11] presented a detailed theoretical analysis of thermo-optic effects associated with the influence of cross-sectionally inhomogeneous heating and induced mechanical stress on the refractive index profile, birefringence, and mechanical strength of active fibres, that is, effects typical of conventional active elements based on doped crystals and glasses. According to their results, the laser output power limit in most configurations of active fibres depends primarily on the fibre core temperature, which is determined by the heat removal effectiveness.

When cooling is performed under natural convection, there is an optimal radius of the outer polymer cladding [12]: $R_0 = k_{\text{pol}}/h^T$, where k_{pol} is the thermal conductivity of the polymer and h^T is the convective heat transfer coefficient on the polymer–air interface. This radius corresponds to the minimal thermal resistance of the polymer cladding and convective heat transfer layer. If there is a radiator with high thermal conductivity, the temperature increase is determined to a significant degree by the thermal contact resistance at the fibre–coolant interface [13]. The main limiting factor is then the thermal degradation (ignition) temperature of the polymer coating.

Yan et al. [16] evaluated the thermal radiation contribution to the cooling of active fibre under lasing conditions. According to their numerical calculations, the radiative heat transfer coefficient is comparable to the convective one when the polymer cladding temperature exceeds 300 °C and the emission spectral density has a maximum in the range 2.5–3 μm. This casts doubt on whether the thermal radiation contribution should be taken into account because it is only significant at temperatures above the damage threshold of the polymer cladding.

At the same time, relatively few experimental studies have been concerned with fibre temperature measurement and active-medium heating in fibre lasers of different configurations. It is worth noting recent work by Jeong et al. [17], who measured the temperature of the active fibre in a high-power Yb–Er codoped fibre laser using a fibre Bragg grating sensor array brought into thermal contact with the active fibre. The sensor temperature was determined from the variation of the reflection spectrum of a probe beam, and the core and cladding temperatures were calculated numerically.

Theoretical analysis of thermal effects in lasers, using the heat equation and appropriate boundary conditions, typically builds on a number of assumptions as to the model system and quantities involved. In this context, an important issue is the ability to directly measure the temperature of the active medium and thermal distortions of laser parameters. Many thermal imaging, interferometric and polarisation techniques for temperature and stress measurements in active elements have been tested in experiments with bulk solid-state lasers [18, 19]. In high-power fibre lasers, the geometry of the active medium and the cooling system hinder contact measurements, and techniques that employ thermal radiation have insufficient spatial resolution. In this study, a fibre interferometer was used in temperature measurements. We measured the net change in the phase of probe light, associated with the temperature-induced index change, over the entire length of an active fibre.

Under optical pumping, refractive-index changes in the fibre core may be caused by two mechanisms: the heating of the active fibre owing to the difference between the pump and laser photon energies (Fig. 1) and the change in the polarisation of the active medium (at optical frequencies) in response to changes in laser level populations [6].

In the latter mechanism, the optical pumping-induced changes in electron level populations lead to changes in the polarisability of the active ion, which entail a local index change proportional to the excited-state population. When the lasing threshold is reached, the population inversion takes on a steady-state value, which enables the temperature to be determined interferometrically under lasing conditions.

Note that the physical processes responsible for index changes differ in timescale, which can be used to separate their contributions in kinetic measurements. From index change kinetics, one can assess the temperature difference between the core and polymer cladding of active fibres and the thermal properties of the polymer [20, 21].

We measured the steady-state temperature of the core in a fibre laser as a function of pump power for various heat removal conditions below and above the lasing threshold using an interferometric technique and probe light of wavelength far away from the absorption edge of the active ion [22]. The probe light source was a distributed-feedback (DFB) semiconductor laser. After passing through a 50/50 fibre coupler, the probe signal was directed to the two arms of a Mach–Zehnder interferometer. One of the arms was the cavity of a fibre laser based on the active fibre to be studied. The DFB lasers used as probe light sources had the following parameters: wavelengths, 1564 and 1304 nm; emission bandwidths, 2 and 30 MHz; coherence lengths,

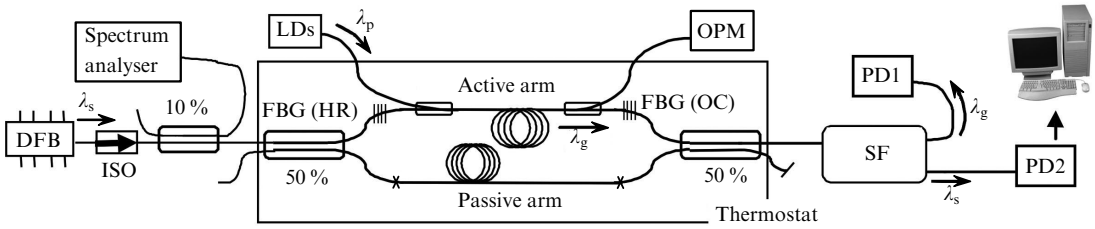

Figure 2. Schematic of the experimental setup: LDs, pump diodes (λ_p); DFB, probe light source ($\lambda_s = 1564$ or 1304 nm); ISO, optical isolator; $\lambda_{laser} = 1064$ or 1540 nm, laser wavelength; OPM, optical power meter; PD1 and PD2, photodetectors; FBG (HR) and FBG (OC), highly reflective and output fibre Bragg gratings; SF, spectral filter separating the probe signal from the laser output.

103 and 7 m, respectively. The former laser had a polarisation-maintaining output fibre pigtail, and the latter had an SMF-28 single-mode fibre pigtail.

The index change induced by optical pumping of the active medium in one of the arms entails a change in the optical path difference for the probe beam and, accordingly, in the output intensity of the interferometer:

$$I_{out} \sim I[1 + \cos \Delta\varphi(t)], \quad (1)$$

where $\Delta\varphi(t)$ is the time-dependent phase difference.

Our experimental setup is shown schematically in Fig. 2.

The 1.3-μm DFB laser, used in our experiments with erbium-doped fibre, has a coherence length comparable to the fibre cavity length. For this reason, when the interferometer arms are longer than 10 m, several longitudinal modes of the cavity formed by perpendicularly cleaved fibre ends of the output coupler may be generated within the gain band of the semiconductor laser, introducing time-domain distortion into the interference pattern. Therefore, one should suppress the reflection of the signal from the cleaves (using an optical isolator or angle cleaving) and monitor the probe light spectrum (we used optical homodyne detection).

Isotropic single-mode fibre interferometers with arm lengths within several metres are extremely sensitive to pressure and temperature variations owing to both the direct influence on the effective mode refractive index and the change in polarisation state. Therefore, to stabilise the interference pattern, the optical system of the interferometer should be placed in a thermally insulated thermostat (Fig. 2).

The measurement procedure is as follows: after a steady state is reached at a given pump power, the corresponding total phase shift is measured. The measurement details and the calibration results obtained by externally heating one of the arms (active or passive) were reported elsewhere [22]. As an example, Fig. 3 shows the time variation of the interference signal for ytterbium-doped fibre.

The temperature coefficient of the refractive index for silica glass is $dn/dT = 10^{-5} K^{-1}$ [23]. When different active fibres were calibrated, this coefficient varied within 10 %, so in what follows we use reference data.

We studied both Yb^{3+} doped and Yb^{3+}/Er^{3+} codoped fibres. Their parameters are listed in Table 1.

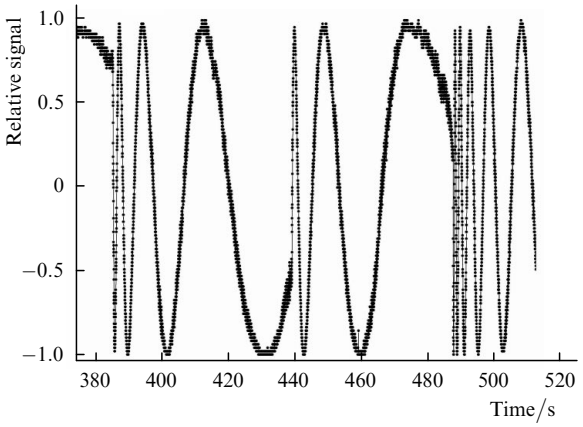

Figure 3. Time variation of the interference signal in response to stepwise changes in pump power at about 385, 440 and 487 s.

Experiments with the ytterbium-doped fibres were conducted under different cooling conditions: the fibres were cooled by air or water under natural convection or placed in a fibre block and potted with a heat-conductive polymer. The experimental results for the ytterbium-doped fibres are presented in Fig. 4. The length-averaged temperature increase in the active fibre as a function of absorbed pump power, P, under lasing conditions (Fig. 4a) can be approximately represented by a linear function of the form $f(P) = mP + f_0$, where m is the slope of the line.

As seen in Fig. 4a, $\Delta T_{mean}(P)$ exhibits nonlinear behaviour near the lasing threshold in the experiment with a fibre block: the slope drops by a factor of 1.5 just above the threshold. The other curves are also nonlinear near the threshold. As an illustration, Fig. 4b presents the differences between the curves and their best fit lines in the form

$$\Delta T_{rel} = \frac{\Delta T(P) - f(P)}{m}. \quad (2)$$

The measurement results for an Yb^{3+}/Er^{3+} codoped fibre under convective air cooling conditions are presented in Fig. 5 as the length-averaged temperature increase against absorbed pump power, together with phase change kinetics in response to pump power switching corresponding to the oscillations in Fig. 3.

Table 1. Parameters of the fibre lasers.

Active medium	Length/m	Ion concentration/ppm	Core radius/μm	Pump wavelength/nm	Pump absorption coefficient/dB m^{-1}	$\Delta n/10^{-3}$	Transmittance of the FBG (OC)/dB
Yb^{3+}	4	4200	5	968	1.2	12.5	−5.5
Yb^{3+}/Er^{3+}	7	5700/173	6.8	972	1.9	16	−5.9

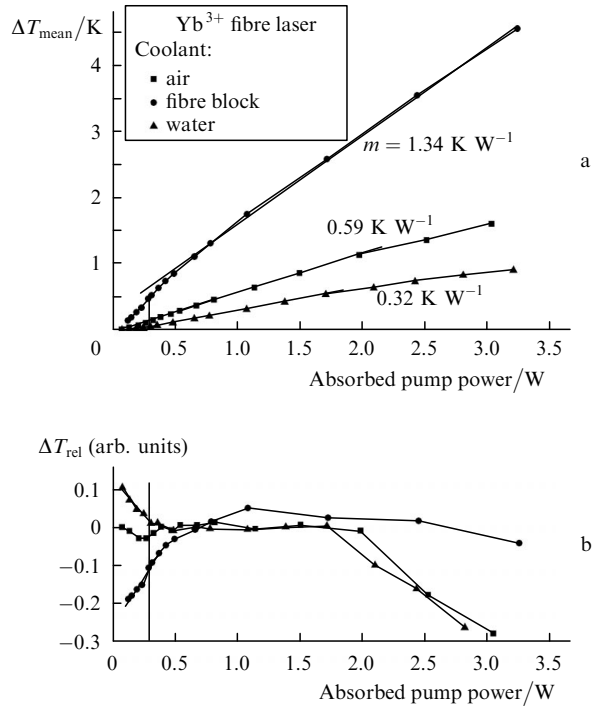

Figure 4. (a) Length-averaged temperature increase and (b) relative fibre heating (relative difference between the experimental curve and its best fit line) as functions of absorbed pump power for the ytterbium fibre laser under different cooling conditions. The vertical lines show the lasing threshold.

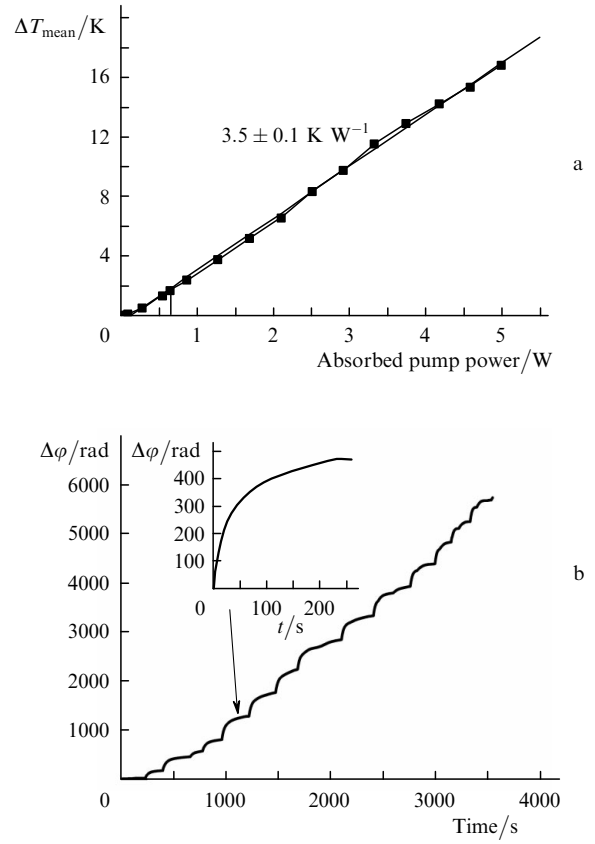

Figure 5. (a) Fibre-length-averaged temperature increase as a function of absorbed pump power and (b) phase difference as a function of time for the Yb^{3+}/Er^{3+} codoped fibre laser. Inset: portion of the curve (indicated by the arrow) plotted from the origin on expanded scales.

It follows from Figs 4a and 5a that the curves for the ytterbium- and erbium-doped fibres under convective cooling conditions differ in slope by a factor of 5.9, which is roughly equal to the ratio of the quantum energy defects for these active media.

The time dependence of the phase difference can be fitted to an equation of the form

$$\Delta\varphi(t) = A_1[1 - \exp(-1/\tau_1)] + A_2[1 - \exp(-1/\tau_2)] + at, \quad (3)$$

where the constant a characterises slow heating of the thermostat. The characteristic times for different 'steps' fall in the ranges $\tau_1 = 2.5 - 7$ s and $\tau_2 = 20 - 30$ s.

We assume that the first term in (3) represents the formation of a quasi-steady-state temperature profile in the fibre and that the other terms are related to the heating of the coolant and thermostat. 'Quasi-steady state' is here taken to mean that the cross-sectional temperature nonuniformity in the fibre is much less that the magnitude of the temperature and that the time needed for a nonuniformity to develop is considerably shorter than τ_1 and τ_2 [14].

To evaluate the rate of heat removal from an axisymmetric active fibre made up of a doped core of diameter d, silica cladding of radius r_0, and polymer cladding of radius b (Fig. 6), we use the heat balance equation

$$\left(c_v^{qu}A_{clad} + c_v^{pol}A_{pol}\right)\frac{d\Delta T}{dt} = \eta Q A_{core} - h^T l \Delta T, \quad (4)$$

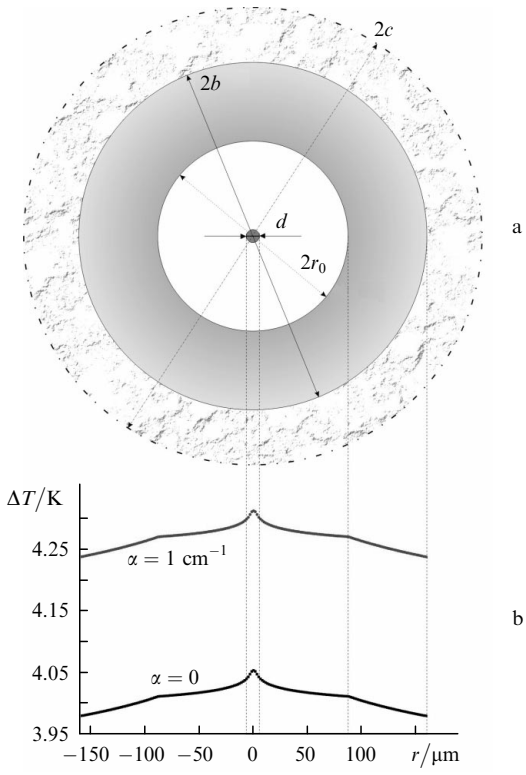

Figure 6. (a) Cross-sectional fibre geometry (d is the diameter of the doped core, r_0 is the radius of the silica glass cladding, and b is the outer radius of the polymer cladding). The four-layer model includes an outer polymer cladding of radius c (indicated by a dot-dashed line not to scale). (b) Radial profile of the fibre temperature increase in a three-layer model. α is the absorption coefficient of the polymer.

where c_v^{qu} and c_v^{pol} are the volumetric heat capacities of quartz glass and the polymer, respectively; A_{clad}, A_{pol} and A_{core} are the areas of the multimode cladding, polymer cladding and doped core; Q is the pump power absorbed per unit volume; l is the perimeter of the outer cladding; η is the fraction of pump power converted to heat; and ΔT is the difference in temperature between the fibre and ambient medium.

The solution to Eqn (4) has the form

$$\Delta T(t) = \Delta T_{st}[1 - \exp(-l/\tau)], \tag{5}$$

where

$$\Delta T_{st} = \frac{\eta Q A_{core}}{h^T l} \quad \text{and} \quad \tau = -\frac{h^T l}{c_v^{qu} A_{clad} + c_v^{pol} A_{pol}}$$

is the temperature transient time.

In our calculations, we used the following model parameters: $d = 10$ μm, $r_0 = 87.5$ μm, $b = 160$ μm, $\eta = 0.1$, $C_v^{qu} = 2.14 \times 10^6$ J m^{-3} K^{-1} [14] and $C_v^{pol} = 1.33 \times 10^6$ J m^{-3} K^{-1} [24] (Sylgard® 182 polymer).

Using the experimentally determined temperature transient time τ_1, we calculated the heat transfer coefficient on the polymer–air interface: $h^T = 15 - 45$ W m^{-2} K^{-1}.

To interpret the decrease in the slope of one of the curves in Fig. 4a near the lasing threshold, we proposed a coaxial active fibre heating model [25]: spontaneous emission absorption in the polymer coating of a fibre causes further heating and, hence, increases the slope of the average temperature vs. pump power curve below threshold. For simplified quantitative modelling, we use a steady-state heat equation. In the case of emission absorption in the polymer cladding, this has the form

$$\frac{1}{r}\frac{\partial}{\partial r} r \frac{\partial T}{\partial r} + \frac{\eta Q}{k_{qu}} = 0, \quad r < \frac{d}{2}, \tag{6}$$

$$\frac{1}{r}\frac{\partial}{\partial r} r \frac{\partial T}{\partial r} = 0, \quad \frac{d}{2} < r < r_0, \tag{7}$$

$$\frac{1}{r}\frac{\partial}{\partial r} r \frac{\partial T}{\partial r} + \frac{\alpha I_0}{k_{pol}} \frac{r_0}{r} \exp[-\alpha(r - r_0)] = 0, \quad r > r_0, \tag{8}$$

where k_{qu} is the thermal conductivity of quartz glass; α is the absorption coefficient in the wavelength range of spontaneous emission in the polymer coating; and I_0 is the luminescence intensity at $r = r_0$.

We assume that spontaneous emission propagates isotropically and that there is no total internal reflection from the polymer surface.

With the designation $\chi = \alpha I_0 r_0 \exp(\alpha r_0)$, Eqn (8) reads

$$\frac{1}{r}\frac{\partial r}{\partial r} r \frac{\partial T}{\partial r} + \frac{\chi}{k_{pol}} \frac{\exp(-\alpha r)}{r} = 0. \tag{9}$$

The general solution to Eqns (6)–(8) is

$$T_1(r) = -\frac{\eta P}{4k_{qu}} r^2 + C_1, \quad r < \frac{d}{2}, \tag{10}$$

$$T_2(r) = C_2 \ln r + C_3, \quad \frac{d}{2} < r < r_0, \tag{11}$$

$$T_3(r) = d_1 \ln r + \frac{\chi}{\alpha k_{pol}} \mathrm{Ei}(-\alpha r) + d_2, \quad r > r_0, \tag{12}$$

where C_1, C_2, C_3, d_1 and d_2 are constants to be determined from boundary conditions, and $\mathrm{Ei}(x) = \int_{-\infty}^{x} (e^t/t)dt$ is the first-order exponential integral.

As extra parameters for numerical modelling, we take $h^T = 25$ W m^{-2} K^{-1}, $Q = 4(dP/dz)(\pi d^2)^{-1}$, $I_0 = (1 - \eta) \times (dP/dz)/(2\pi r_0)^{-1}$, $k_{qu} = 1.46$ W m^{-2} K^{-1} and $k_{pol} = 0.3$ W m^{-2} K^{-1}.

Figure 6b shows the radial temperature profile in a fibre at absorption coefficients of the polymer for spontaneous emission $\alpha = 0$ and 1 cm^{-1}.

To more generally describe the temperature distribution at the fibre surface, the thermal problem geometry should be modified by adding a fourth layer. It is basically the heat-removing and damping polymer in the fibre block, which absorbs the luminescence (Fig. 6a). We take the thermal conductivity of the fourth layer to be $k_4 = 0.2$ W m^{-1} K^{-1} (WACKER SilGel® 612 polymer + 8 % Al_2O_3 [26]) and vary its outer radius.

Figure 7 plots the ratio of the core temperature in the coaxial model to that in a conventional model that neglects the absorption in the cladding against absorption coefficient.

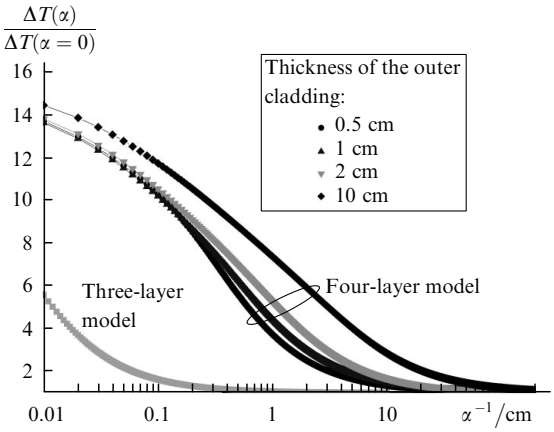

Figure 7. Ratio of the core temperature in a three-layer geometry to that in a four-layer geometry as a function of effective absorption length at different radii of the outer cladding.

Note that this ratio is independent of pump power because in both cases it appears as a factor in all expressions for the temperature. As seen in Fig. 7, the fibre temperature in the three-layer model increases markedly only at rather large absorption coefficients ($\alpha > 10$ cm^{-1}), in contrast to common practice. When there is an extra polymer cladding of radius comparable to the thickness of the fibre block used in our experiments (about 0.5 cm), the temperature of the fibre and adjacent polymer increases twice as much even at $\alpha = 0.2 - 0.33$ cm^{-1}.

When there is no outer polymer cladding, the increase in the slope of the $\Delta T = f(P)$ curve above the lasing threshold is due to the fact that the wavelength-averaged effective quantum energy defect in the case of spontaneous emission is smaller in comparison with stimulated 1064-nm emission. The increase in slope is more pronounced in the case of water cooling and is insignificant in the case of air cooling (Fig. 4).

The effective quantum defect can be evaluated from the spectral dependence of the emission cross section for the active ion. The spectral power density of spontaneous emission is related to the emission cross section by [27]

$$P_{\mathrm{lum}} \sim \sigma_{\mathrm{em}}(\lambda)/\lambda^5. \quad (13)$$

Normalising this expression to unity, we can find the photon down-conversion efficiency as a function of pump wavelength. The data derived from the measured Yb^{3+} cross section in phosphosilicate glass fibres [27] are presented in Fig. 8.

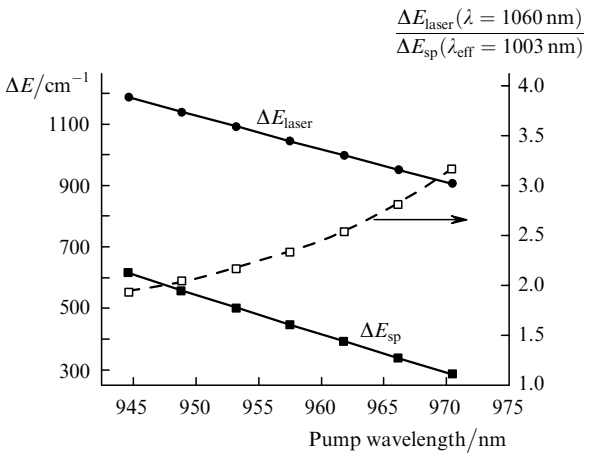

Figure 8. Quantum energy defect as a function of pump wavelength for spontaneous emission (■) and 1060-nm stimulated emission (●) and the ratio of the quantum defects (□).

The effective spontaneous emission wavelength, λ_{eff}, in the case under consideration is ~ 1003 nm. Anti-Stokes luminescence under excitation at wavelengths above λ_{eff} is used in solid-state laser cooling [28]. Under ideal conditions, the ratio of the quantum energy defects for spontaneous and stimulated emission should be equal to the ratio of the slopes of the curves in question below and above the lasing threshold. Under the experimental conditions of this study, this feature is smoothed away by several factors. These include partial pump absorption in the polymer coating of the fibre and amplified spontaneous emission, which further reduces the inversion in the extended active medium and raises the fibre temperature. In addition, part of the spontaneous emission propagates along the multimode waveguide formed through total internal reflection from the polymer surface and is absorbed more efficiently. The numerical aperture of such a waveguide will be smaller in the case of water cooling (the refractive index of water is 1.33), so the increase in slope will be more pronounced.

In general, the thermal performance of an active fibre at low pump powers near the lasing threshold is determined by a combined effect of the above factors.

The case of high pump powers is of considerable interest. With increasing power, one would expect a deviation from linearity in the variation of the fibre temperature with pump power (as observed even at the medium pump powers used in our experiments, see Fig. 4) because the heat transfer coefficient h^T depends on the temperature difference across the fibre surface. The similarity relation for natural convection in the case of horizontal cylinders has the form [29]

$$\overline{\mathrm{Nu}} = 0.36 + \frac{0.518(\mathrm{Gr}\,\mathrm{Pr})^{1/4}}{\left[1 + (0.559/\mathrm{Pr})^{9/16}\right]^{4/9}}, \quad (14)$$

where $\overline{\mathrm{Nu}} = h^T D/k_{\mathrm{air}}$ is the Nusselt number; $\mathrm{Pr} = v/\varkappa$ and $\mathrm{Gr} = g\beta\Delta T D^3/v^2$ are, respectively, the Prandtl and Grashof numbers of the coolant; $D = 2b$ is the fibre diameter; v is kinematic viscosity; $\varkappa = k/c_v$ is thermal diffusivity; β is volume expansivity; and g is the standard acceleration of gravity. The Prandtl number of air at 290 K is $\mathrm{Pr} = 0.54$. With appropriate parameters, relation (14) takes the form

$$\overline{\mathrm{Nu}} = 0.36 + 0.049\sqrt[4]{\frac{\Delta T}{1K}}. \quad (15)$$

At a small temperature difference, the second term can be neglected, and the heat transfer coefficient estimated for the geometry in question is $h^T \approx 58\ \mathrm{W\ m^{-2}\ K^{-1}}$, which exceeds the experimentally determined values. In a real situation, the fibre is bent into a coil, which hinders the heat removal, gives rise to local overheating, and reduces the effective heat transfer coefficient.

In addition to the fourth root variation of the heat transfer coefficient with the temperature difference across the fibre surface [see Eqn (15)], a certain contribution can be made by the temperature dependence of the thermal parameters (viscosity, heat capacity and thermal conductivity) of the environment.

We plan to perform temperature measurements at high pump and output powers, in which limitations will be imposed by the optical damage threshold and thermal stability of the optical components involved, primarily by those of a single-mode 50/50 output coupler with stable optical characteristics at optical powers of up to 20 W. In connection with this, it is reasonable to perform measurements at high powers using a Michelson interferometer, which allows one to observe interference of probe light reflected from a perpendicularly cleaved active-fibre end, or using an appropriate anti-reflection coated collimating lens.

Thus, the thermal effects in fibre lasers were studied experimentally using interferometric temperature measurements in the core of the active fibre under high-power optical pumping. We measured the temperature of Yb^{3+} and Er^{3+} doped fibres at pump powers of up to 15 [22] and 5 W, respectively, at different pump wavelengths. The average fibre temperature was found to be a nonlinear function of absorbed pump power near the lasing threshold. The nonlinearity is governed by the optical and thermal properties of the polymer coating and luminescence conditions of the active medium. A coaxial heating model was proposed, and the influence of the effects in question on the temperature of the active medium was evaluated using numerical calculations. From the observed kinetics of active-fibre heating under convective air cooling conditions, we estimated the heat transfer coefficient on the polymer–air interface for a given fibre geometry. The numerical data thus obtained can be useful in modelling the thermal conditions of fibre laser operation, in particular, at high output powers.

References

1. Woods S., Duka M., Flinn G. *Fotonik Int.*, **1**, 46 (2006).

2. Gapontsev V.P., Samartsev I.E., in *OSA Proc. on ASSL* (Salt Lake City, 1990) Vol. 6, p. 258.
3. Fomin V., Abramov M., Ferin A., et al., in *Abstracts 14th Intern. Conf. Laser Optics 'LO-2010'* (St.Petersburg, 2010) TuSy-1.3.
4. Dawson J.W., Messerly M.J., Beach R.J., et al. *Opt. Express*, **16**, 13240 (2008).
5. Boulon G. *J. Alloys Compd.*, **451**, 1 (2008).
6. Digonnet M.J.F., Sadowski R.W., Shaw H.J., Pantell R.H. *Opt. Fiber Technol.*, **3**, 44 (1997).
7. Van den Hoven G.N., Snoeks E., Polman A., et al. *J. Appl. Phys.*, **79**, 1258 (1996).
8. Jeong Y., Yoo S., Codemard C.A., Nilsson J., et al. *IEEE J. Sel. Top. Quantum Electron.*, **13**, 573 (2007).
9. Vyatkin M.Yu., Grabarnik S.P., Ryabushkin O.A. *Kvantovaya Elektron.*, **35**, 323 (2005) [*Quantum Electron.*, **35**, 323 (2005)].
10. Brilliant N.A., Lagonik K. *Opt. Lett.*, **26**, 1669 (2001).
11. Brown D.C., Hoffman H.J. *IEEE J. Quantum Electron.*, **37**, 207 (2001).
12. Zintzen B., Langer T., Geiger J., Hoffmann D., Loosen P. *Proc. SPIE–Int. Soc. Opt. Eng.*, **6873**, 687319-1 (2008).
13. Lapointe M.-A., Chatigny S., Piché M., Cain-Skaff M., Maran J.-N. *Proc. SPIE–Int. Soc. Opt. Eng.*, **6873**, 687819-1 (2009).
14. Davis M.K., Digonnet M.J.F., Pantell R.H.J. *Lighwave Technol.*, **16**, 1013 (1998).
15. Yong Wang, Chang-Qing Xu, Hong Po. *IEEE Photonics Technol. Lett.*, **16**, 63 (2004).
16. Yan P., Xu A., Gong M. *Opt. Eng.*, **45**, 124201 (2006).
17. Jeong Y., Baek S., Dupriez P., et al. *Opt. Express*, **16**, 19865 (2008).
18. Mezenov A.V., Soms L.N., Stepanov A.I. *Termooptika tverdotel'nykh lazerov* (Thermo-optics of solid-state lasers) (Leningrad: Mashinostroenie, 1986).
19. Chenais S., Druon F., Forget S., et al. *Prog. Quantum Electron.*, **30**, 89 (2006).
20. Fotiadi A., Antipov O., Megret P. *Opt. Express*, **16**, 12658 (2008).
21. Gainov V., Ryabushkin O.A. *Proc. 3rd EPS–QEOD Europhoton Conf.* (Paris, 2008) THoD.5.
22. Gainov V.V., Shaidullin R.I., Ryabushkin O.A. *Prib. Tekh. Eksp.*, **6**, 86 (2010).
23. Kikoin I.K. (Ed.) *Tablitsy fizicheskikh velichin. Spravochnik* (Tables of Physical Quantities: A Handbook) (Moscow: Atomizdat, 1976).
24. Reinert F., Luthy W. *Opt. Express*, **13**, 10749 (2005).
25. Shaidullin R.I., Gainov V.V., Ryabushkin O.A. *Trudy VII mezhd. konf. 'Lazernaya fizika i opticheskie tekhnologii'* (Proc. VII Int. Conf. on Laser Physics and Optical Technologies) (Minsk, 2008) Vol. 2, p. 461.
26. http://www.wacker.com, http://www.swiss-composite.ch/pdf/t–Silgel-612.pdf.
27. Mel'kumov M.A., Bufetov I.A., Kravtsov K.S., Shubin A.V., Dianov E.M. *Kvantovaya Elektron.*, **34** (9), 843 (2004) [*Quantum Electron.*, **34** (9), 843 (2004)].
28. Petrushkin S.V., Samartsev V.V. *Laser Cooling of Solids* (Sawston: Woodhead, 2009; Moscow: Fizmatlit, 2004).
29. Lienhard J.H. IV, Lienhard J.H. V. *A Heat Transfer Textbook* (Cambridge, MA: Phlogiston Press, 2001).